ACS APPLIED MATERIALS & INTERFACES

Research Article

Cite This: ACS Appl. Mater. Interfaces 2019, 11, 12261−12271

www.acsami.org

Stretchable Micromotion Sensor with Enhanced Sensitivity Using Serpentine Layout

Zhuocheng Yan,[†] Taisong Pan,*[,†] Dengke Wang,[†] Jiacheng Li,[†] Long Jin,[§] Long Huang,[†] Jiahao Jiang,[†] Zhihui Qi,[†] Hulin Zhang,[†,∥] Min Gao,[†,‡] Weiqing Yang,[§] and Yuan Lin*[,†,‡]

[†]State Key Laboratory of Electronic Thin Films and Integrated Devices and [‡]Center for Information in BioMedicine, University of Electronic Science and Technology of China, Chengdu 610054, P. R. China

[§]Key Laboratory of Advanced Technologies of Materials (Ministry of Education), School of Materials Science and Engineering, Southwest Jiaotong University, Chengdu 610031, P. R. China

[∥]MicroNano System Research Center, Key Lab of Advanced Transducers and Intelligent Control System of the Ministry of Education & College of Information and Computer, Taiyuan University of Technology, Taiyuan 030024, P. R. China

Supporting Information

ABSTRACT: The application of the serpentine mesh layout in stretchable electronics provides a feasible method to achieve the desired stretchability by structural design instead of modifying the intrinsic mechanical properties of the applied materials. However, previous works using the serpentine layout mainly focused on the optimization of structural stretchability. In this paper, the serpentine mesh design concept is used to transform the high-performance but hard-to-stretch piezoelectric film into a stretchable form. The serpentine layout design strategies for the piezoelectric film, which aim at not only desired stretchability but also high utilization of the strain in the piezoelectric film during deformation, are discussed with experimental and computational results. A stretchable micromotion sensor with high sensitivity is realized using the piezoelectric film with a serpentine layout. Human voice recognition applications of the sensor, including speech pattern recognition with machine learning, are demonstrated with the sensor integrated with a wireless module. The stretchable micromotion sensor with a serpentine layout illustrates the broader application of serpentine layout design in the functional materials of stretchable electronics, which can further extend the range of available functional materials for novel stretchable electronic devices.

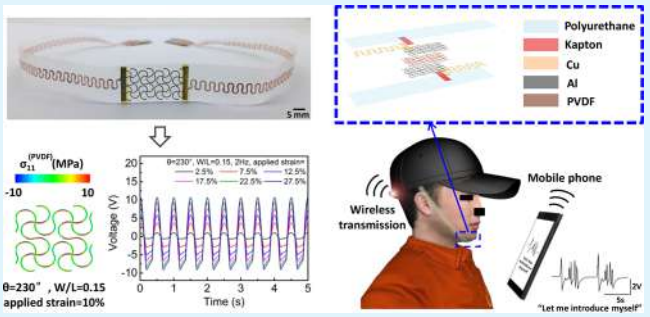

KEYWORDS: *stretchable electronics, serpentine layout, motion sensor, strain sensor, self-powered sensor, piezoelectric, machine learning*

INTRODUCTION

With the rapid development of stretchable electronic devices, various stretchable human motion sensors, which can form conformal contact with human skin to monitor the movement of the human body such as gestures, walking type, and body pose, are proposed in recent research studies.[1−3] These proposed sensors show substantial potential in realizing the human−robot interaction and health monitoring for medical purposes. Besides the large-scale movement, the tiny movements in some parts of the human body are also important signal sources in interdisciplinary studies. One example is the application of throat motion detection in the antinoise voice recognition.[4] In the highly noisy environment, the remote voice communication between people is hard to realize by using microphone directly.[5] With a stretchable motion sensor attached to the skin around the throat, the voice signal can be converted from the detected throat motion signals. As the motion signals are only caused by speaking, it will not be affected by other noise sources. The application of voice recognition can even be extended to the treatment of some diseases like aphasia.[6] In current treatment of aphasia, doctors often use a microphone to record the pattern of speech to evaluate the speech ability of a patient.[7] One major drawback of the microphone-based method is that the voice signal collected by a microphone is vulnerable to the ambient noise. The interference from ambient noise makes it difficult to properly judge the condition of the patient and make a suitable treatment plan with the collected information of the patient's speech ability. The voice recognition based on throat motion, which avoids the potential interference, can provide a reliable signal source to assist the treatment of aphasia. The applications of detecting tiny motions of the human body

Received: December 27, 2018
Accepted: February 26, 2019
Published: February 26, 2019

DOI: 10.1021/acsami.8b22613
ACS Appl. Mater. Interfaces 2019, 11, 12261−12271

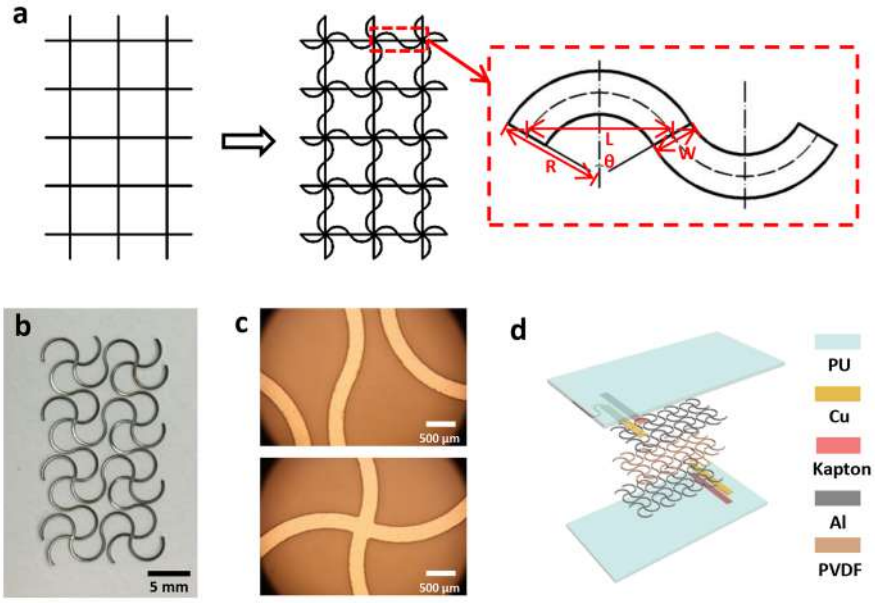

Figure 1. (a) Schematic of the serpentine layout. (b, c) Optical images of the PVDF film with a serpentine layout. (d) Exploded view schematic of the micromotion sensor with a serpentine layout.

require not only a certain level of stretchability of the sensor to ensure conformal contact but also high sensitivity of the sensor to meet the need of tiny movement detection.

To detect the movement of the human body, a common solution is to design a device to detect strain-driven change of a particular electrical signal, such as resistance,[8−15] capacitance,[16−21] and piezoelectric signal.[22−24] For a stretchable device used in the human motion monitoring, miniaturization and long-term stability of performance are significant features. As the piezoelectric micromotion sensor is based on the principle of generating output voltage or current signals depending on the strain, it can work without any external power source.[25] The elimination of the need for batteries can further promote the size reduction of the stretchable device and improve the reliability of the device. Moreover, as the piezoelectric material only has impulsive output voltage or current during the change of strain on the material, the background noise is very small when detecting the dynamic movement of the human body, which can significantly improve the signal-to-noise ratio (SNR) of the sensor.[26]

For the piezoelectric micromotion sensor used to detect the tiny movement of the human body, the strain change is small, which requires the piezoelectric material in the sensor to have a large piezoelectric coefficient so as to generate strong electric signals. However, many piezoelectric materials with large piezoelectric coefficients, such as poly(vinylidene fluoride) (PVDF), have high elastic modulus (e.g. PVDF: ∼2 GPa), which makes them difficult to be directly stretched and applied in the stretchable micromotion sensor. Recent reports on the applications of a serpentine mesh layout in stretchable electronics provide a hint for solving such a difficulty and creating the opportunity to apply the intrinsically hard-to-stretch piezoelectric film in stretchable micromotion sensors.[27−29] By patterning the film to form a mesh layout consisting of serpentine unit cells, desired stretchability can be obtained for the piezoelectric film, which possesses high performance but is intrinsically hard-to-stretch.

Previous researches on the application of the serpentine layout in the stretchable electronics mainly focused on the optimization of stretchability.[30−33] To improve the stretchability, the strain in the functional layer of the serpentine layout needs to be kept below the maximum strain level required for mechanical reliability during stretching. However, for some kinds of functional materials, such as the piezoelectric materials, their output characteristics strongly depend on the strain level in the materials. In many cases, the optimizations of the stretchability and the output characteristics prefer contrary strain levels. For example, to obtain a high output voltage or current, the layout should be designed to maximize the strain level in the piezoelectric layer when being stretched. On the contrary, to achieve high stretchability, the strain coupled on the hard-to-stretch function layer should be as low as possible to avoid cracking. In other words, challenges exist in the layout design of the micromotion sensor based on the functional materials, which needs not only to meet the mechanical stretchability requirements but also to optimize the output characteristics such as the output voltage at a certain stretchability level.

In this study, a stretchable micromotion sensor used to monitor the movement of the throat is designed and fabricated with a serpentine mesh geometric piezoelectric film. With the systematic study on the correlations between geometric parameters, stretchability, and output piezoelectric voltage, the design strategy for the serpentine layout in the stretchable piezoelectric micromotion sensor is presented. The optimized serpentine layout can utilize the transverse piezoelectric effect more effectively to provide a larger output piezoelectric voltage and meet the mechanical stretchability requirement. By attaching the sensor on the skin near the throat, the movement of the throat can be captured by the electric voltage signal associated with the strain of the skin. Combining the wireless signal recording and the analysis with the machine learning approach, the application of the stretchable human micromotion sensor in spoken word recognition is also demonstrated.

DOI: 10.1021/acsami.8b22613
ACS Appl. Mater. Interfaces 2019, 11, 12261−12271

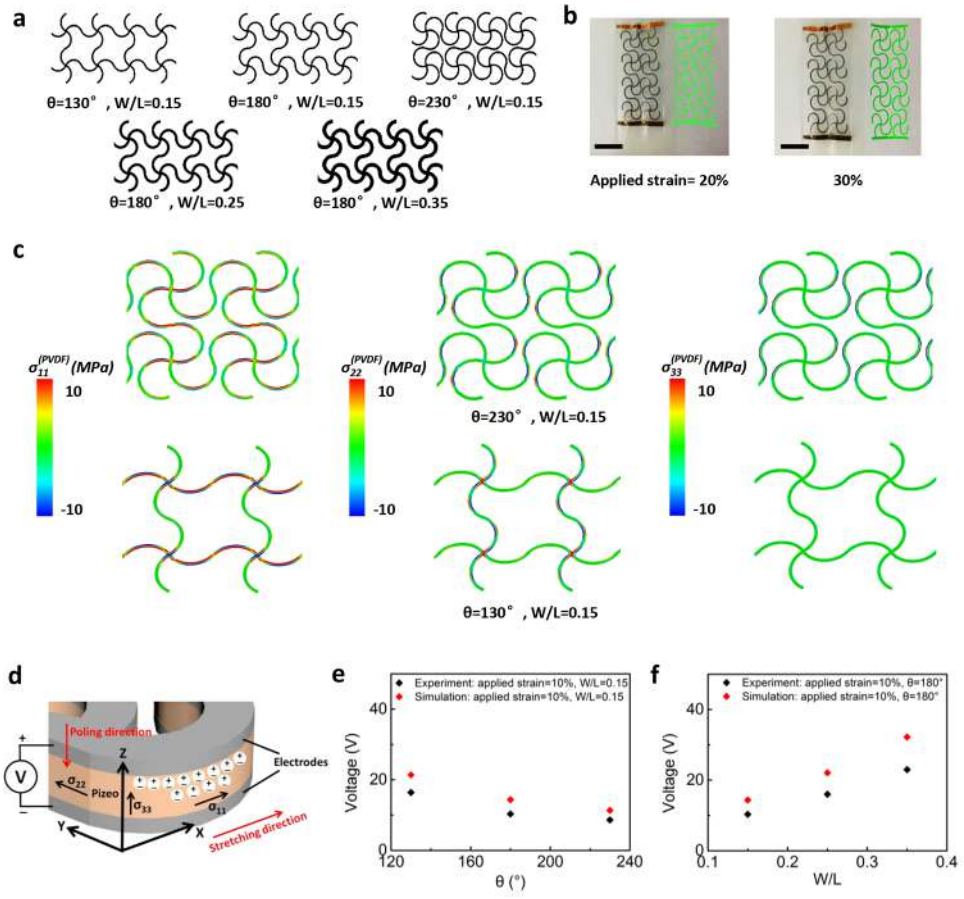

Figure 2. Mechanism analysis of the stretchable micromotion sensor with a serpentine layout. (a) The schematic illustrations of the serpentine layouts with different arc angles θ and W/L ratios. (b) Optical images (left) and FEA (right) deformation results of the encapsulated PVDF film with a serpentine layout under different uniaxial tensile strains (scale bar: 10 mm). (c) σ_{11}, σ_{22}, and σ_{33} distribution in the PVDF layer of the sensor with θ of 230 (top) and 130° (bottom), W/L of 0.15, and applied strain of 10%. The corresponding zoomed-in figures of the stress concentration areas are shown in Figure S3 of the Supporting Information. (d) Schematic illustrations of the basic working mechanism of the sensor. (e) Computational and experimental results of open-circuit voltages of the sensors with fixed W/L of 0.15 and different arc angles θ (applied strain = 10%). (f) Computational and experimental results of open-circuit voltages of the sensors with a fixed arc angle θ of 180° and different W/L (applied strain = 10%).

RESULTS AND DISCUSSION

Figure 1a presents the schematic illustration of the serpentine layout in this study. The structure is based on a mesh geometry, which consists of serpentine unit cells along the vertical and horizontal directions. Each serpentine unit cell includes two identical circular arcs with the same arc angle, radius, width, and span. The key geometric parameters include the arc angle (θ), the radius (R), and the width (W). The relationship between R and θ is given by

$$\theta = 2\sin^{-1}\frac{L}{2R} \quad (1)$$

where L is the span or the chord length. For consistency of discussion, L is fixed to 2 mm in this study. Using the cutting method (see the Experimental Section for the details), the piezoelectric film, consisting of stacked layers of a bottom metal layer (Al, 6-μm-thick), a piezoelectric PVDF layer (110-μm-thick), and a top metal layer (Al, 6-μm-thick), is processed to form the serpentine mesh geometry. Figure 1b and Figure S1 in the Supporting Information show that the cutting method can well define the serpentine layout in the film. The zoomed-in images shown in Figure 1c and Figure S2 in the Supporting Information also indicate that there is no crack on the film cut with the serpentine layout and the edges are uniform and smooth. To form the micromotion sensor, the top/bottom metal layers of the geometry-defined piezoelectric film are connected with wires made of 50-μm-thick Cu foil. Then, the whole unit and the wires are encapsulated by two layers of thin polyurethane (PU) membranes (47-μm-thick), as illustrated in Figure 1d. The Kapton tape is utilized to ensure physical contact between the Cu foil and the piezoelectric film.

For a piezoelectric sensor, the output performance of the sensor is closely related to the stress (strain) in the piezoelectric material (the PVDF layer of the sensor in our study). To understand the influence of serpentine layout geometric parameters on the output performance of the piezoelectric micromotion sensor, the stress (strain) distribution in the PVDF layer was analyzed. By using the finite element analysis (FEA), we evaluated the stress distribution in the PVDF layer of the micromotion sensor with different serpentine layout geometric parameters. As shown in Figure 2a, five geometry parameter configurations, which can be classified by the geometric parameters θ and W/L, were studied in the FEA. Quantitative agreements between the

DOI: 10.1021/acsami.8b22613
ACS Appl. Mater. Interfaces 2019, 11, 12261−12271

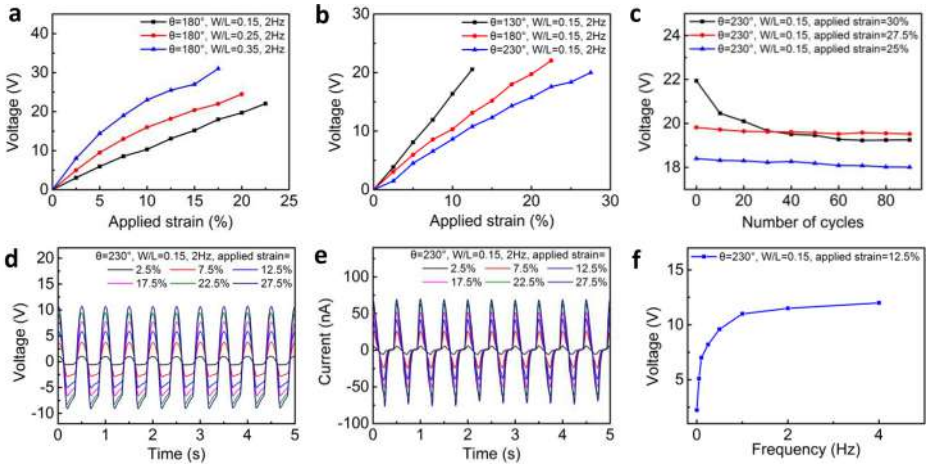

Figure 3. Output measurement of the stretchable micromotion sensor with a serpentine layout. (a) Open-circuit voltages of the sensors with different arc angles θ and applied strains. (b) Open-circuit voltages of the sensors with different W/L ratios. (c) Open-circuit voltages of the sensor with different cycling numbers (θ = 230°, W/L = 0.15, 2Hz). (d, e) Open-circuit voltages and short-circuit currents under different applied strains (θ = 230°, W/L = 0.15, 2Hz). (f) Open-circuit voltages of the sensor under stretching with different frequencies (θ = 230°, W/L = 0.15, 2Hz).

physical deformations in experiments and the ones in FEA results were observed throughout the entire range of stretching (applied strain of 20 and 30%), as indicated by Figure 2b. Figure 2c and Figure S3 of the Supporting Information show the distributions of stress in the x, y, and z directions in the piezoelectric layer (PVDF layer) with two different serpentine layouts and 10% applied strain (top panel: θ = 230° and W/L=0.15; bottom panel: θ = 130° and W/L = 0.15), which are derived from the FEA results. The stress distributions of the other geometry configurations are demonstrated in Figures S4 and S5 of the Supporting Information. The simulation results clearly indicate the existence of stress concentration when stretching the PVDF layer with a serpentine layout, which is similar to previous studies on the serpentine layout structure.[34] Stress concentration regions can be found in the arc segments of the serpentine unit cell, especially for σ_{11} and σ_{22}. The uneven distribution of stress leads to the gradient polarization in the z direction, which causes a significant difference on the amount of surface charges between the arc segment and the remaining segments of the serpentine structure. Moreover, as shown in Figure 2c, the stress distribution in the PVDF layer closely depends on the geometric parameters of the serpentine layout. With the same 10% applied tensile strain, the stress distribution is different in the PVDF layer when varying the geometric parameters. As illustrated by Figure 2d, when the sensor is stretched, the stresses along the x, y, and z directions in the piezoelectric layer, caused by the bending and tension of the serpentine layout, lead to the shift of the positive and negative charge centers. At the same time, a voltage drop can be measured between the top and bottom surfaces of the piezoelectric layer.

As indicated by the FEA results, obvious geometry dependence and the stress concentration effect of the stress distribution can be observed in the stretched piezoelectric film with the serpentine layout. These effects make it difficult to evaluate the output performance of the piezoelectric film with the serpentine layout based on the level of applied tensile strain only. It is necessary to further investigate the influence of the serpentine layout geometry on the piezoelectric output properties by estimating the surface charge distribution in the view of stress distribution. Therefore, we propose a theoretical model based on piezoelectric constitutive equations to calculate the open-circuit (OC) voltage of the piezoelectric micromotion sensor with the serpentine layout. The calculation starts from estimating the surface charge in the unit area of the film with the serpentine layout, corresponding to the stress in the x (σ_{11}), y (σ_{22}), and z directions (σ_{33}). The piezoelectric constitutive equation for the piezoelectric surface charge in the x–y plane in each unit area (dQ) can be written as[35]

$$dQ = [d_{31}, d_{32}, d_{33}] \cdot \begin{bmatrix} \sigma_{11} \\ \sigma_{22} \\ \sigma_{33} \end{bmatrix} \cdot dS \tag{2}$$

where dS is the unit area of the film, and d_{31}, d_{32}, and d_{33} are the piezoelectric charge coefficients of the piezoelectric material in the x, y, and z directions, respectively. The OC voltage (V) with thickness h can be obtained by integral calculation, which is given by[35]

$$V = \sum_{i=1}^{3} \cdot \int \frac{d_{3i}\sigma_{ii}dS}{\frac{\varepsilon_{ii}}{h}dS} = \sum_{i=1}^{3} h \cdot \int \frac{g_{3i}\sigma_{ii}(x, y)dS}{dS} \tag{3}$$

where ε_{11}, ε_{22}, and ε_{33} are the dielectric constants of the piezoelectric material in the x, y, and z directions, respectively, and g_{31}, g_{32}, and g_{33} are the piezoelectric voltage constants of the piezoelectric material in the x, y, and z directions, respectively. The detailed process and parameters of the calculation are illustrated in the calculation section of the Supporting Information.

Based on eqs 1 and 2, the OC voltages of the piezoelectric layer of the micromotion sensor in our study (PVDF layer), with different geometric parameters, are calculated with the strain values derived from the FEA results. Figure 2e,f illustrates the calculated correlations between the geometric parameters and OC voltage of the sensor. With larger stress indicated by the FEA results, the PVDF layer with a larger ratio of width/chord length or a smaller arc angle can generate a higher OC voltage when it is stretched. We also fabricated the sensors corresponding to the five serpentine layout geometry configurations and measured the OC voltage experimentally. The calculated results are consistent with the experimental ones, which show that the proposed model can be used to

DOI: 10.1021/acsami.8b22613
ACS Appl. Mater. Interfaces 2019, 11, 12261−12271

effectively evaluate the output performance of the piezoelectric film with the serpentine layout. However, the calculated OC voltage is slightly higher than the one measured from the experiments, which may be caused by the electric contact type between the metal electrodes and the PVDF film and the defects in the Al/PVDF/Al sandwiched film.[36] The Schottky barriers in the Al/PVDF/Al interface, which can be observed in the $I-V$ curve (Figure S6 of the Supporting Information), hinder the electrons from being transported through the interface and lead to the decrease of output voltage.[37] The defects in the interface between the Al and PVDF layers, such as the gaps in the Al/PVDF interface indicated by the cross-sectional SEM image (Figure S7 of the Supporting Information), would also affect the transport of electrons through the interface. Nevertheless, the theoretical and experimental studies on the design of the serpentine layout for the piezoelectric film clearly shows that the geometric parameters of the serpentine layout, including the ratio of width/chord and the arc angle, play a key role in determining the output performance by affecting the stress (strain) distribution in the film.

Figure 3a,b summarizes the detailed test results of the output performance of the sensors with the five serpentine layout configurations shown in Figure 2a. Figure 3a shows the measured correlation between the output OC voltage and the applied strain with the arc angle θ ranging from 130 to 230° and a fixed W/L = 0.15. Besides the obvious trend that the output OC voltage of each as-fabricated micromotion sensor increases with a larger applied tensile strain, significant influence of the arc angle value on the output OC voltage is observed. When stretching the sensors with the same level of tensile strain, the output OC voltage increases with the decrease of the arc angle from 230 to 130°. A similar phenomenon can also be observed when varying W/L with a fixed θ. As demonstrated in Figure 3b, the output OC voltage increases with a higher value of W/L when the applied strain is the same. Moreover, the similar trend with varied θ and W/L can also be observed in the correlation between the applied tensile strain and the output short-circuit (SC) current illustrated in Figure S8 of the Supporting Information. The dependence of the output performance on the geometry parameters with different applied strains further confirms that the strain distribution in the piezoelectric material is highly relevant to the geometry of the serpentine layout. However, the test results shown in Figure 3a,b also indicate that although decreasing θ and increasing W/L can improve the output performance of the sensor, these modifications of geometric parameters lead to lower stretchability. The sensor with a fixed W/L = 0.15 can be stretched to 27.5% when θ is 230°, whereas the stretchability can only reach 12.5% when θ decreases to 130°. When changing the W/L value from 0.35 to 0.15 with a fixed θ = 180°, the stretchability of the sensor decreases from 22.5 to 17.5%. When the applied strain is higher than the stretchability of the sensor, a gradual decrease of OC voltage can be observed. Figure 3c shows the OC voltage of the sensor, with geometric parameters θ = 230° and W/L = 0.15, during 90 cycles of stretching with applied tensile strains from 25 to 30%. When the applied strain was higher than 30%, the OC voltage started to decrease after 10 cycles, which may be caused by the aging effect of PVDF with excessive strain. According to the measured strain−stress curve of the PVDF layer of the film used in our work (Figure S9, Supporting Information), the PVDF layer can easily yield when the strain in PVDF film is higher than 5%. When the applied strain is 30%, the largest maximum principle strain in PVDF layer indicated by FEA results is more than 5%, and the excessive strain may lead to damages in the PVDF layer and cause the gradually decrease of output voltage, as reported by another work.[38] The contrary preference for stress in the optimization of stretchability and output performance arises a trade-off consideration in the design of the serpentine layout for the piezoelectric film. Pursuing higher stretchability by applying a serpentine layout, which merely reduces the stress in the piezoelectric layer, would lead to poorer output performance of the device. For a stretchable sensor expected to be attached to the human skin, the stretchability of the sensor should be ~30%.[39] The geometric parameters of the serpentine layout need to be carefully chosen to meet both the required stretchability and the reliable signal strength level. According to the measurement results shown in Figure 3c, when θ = 230° and W/L = 0.15, the stretchability of the sensor with the serpentine mesh geometry can reach 27.5%, which can meet the required stretchability for attaching on the human skin. Moreover, the strain in the Al layer of the Al/PVDF/Al film used in sensor fabrication (θ =230°, W/L=0.15) was derived from the FEA result (Figure S10 of the Supporting Information). When the applied strain is 27.5%, the largest maximum principle strain in the Al layer is ~2%, which is much smaller than the fracture strain of metal (~5%).[40] Both the simulated strain distribution of the Al layer and the experimentally output results with cyclic stretching confirm the mechanical reliability considering the cyclic stretching.

Further experiments were conducted to confirm the feasibility of this geometric configuration in the application of human micromotion sensors. As presented in Figure 3d,e, the output OC voltage and SC current of the micromotion sensor with the geometric configuration of θ = 230° and W/L = 0.15 were recorded when the sensor was stretched cyclically with different levels of applied tensile strains. Stable output performance was observed during the cyclic loading (2 Hz). The peak−peak value of the output OC voltage and the output SC current reached up to 19.8 V and 75 nA, respectively. The output OC voltage is large enough to drive two LEDs (Movie S2 in the Supporting Information). Besides the high output values, the sensitivity of the micromotion sensor is another vital parameter that should be considered, which can be defined as[41,42]

$$\text{Sensitivity} = \frac{\Delta V}{\Delta L/L_0} \text{ or } \frac{\Delta I}{\Delta L/L_0} \tag{4}$$

where ΔV is the relative change in the output OC voltage, ΔI is the relative change in the output SC current, ΔL is the length change of the sensor, and L_0 is the original length of the sensor; $\varepsilon = \Delta L/L_0$ denotes the applied strain of the sensor. According to eq 4, the sensitivity of the serpentine mesh geometric micromotion sensor with the geometric configuration θ = 230° and W/L = 0.15 is determined to be 72 V/ε and 272.73 nA/ε at 2 Hz (size of 3.0 cm × 1.6 cm × 0.216 mm), which are higher than the reported values of flexible piezoelectric sensors based on $BaTiO_3$ nanofibers (~0.93 V/ε at 2 Hz, size of 4.5 cm × 2.0 cm × 0.5 cm)[42] and the reported value of ZnO nanowire films grown on the surface of the elastic wire for a spring (~0.95 V/ε and 25.4 nA/ε, size of 5.08 cm × 0.79 cm × 0.79 cm).[43] The frequency dependence of the output OC voltage was also measured with the geometric

DOI: 10.1021/acsami.8b22613
ACS Appl. Mater. Interfaces 2019, 11, 12261−12271

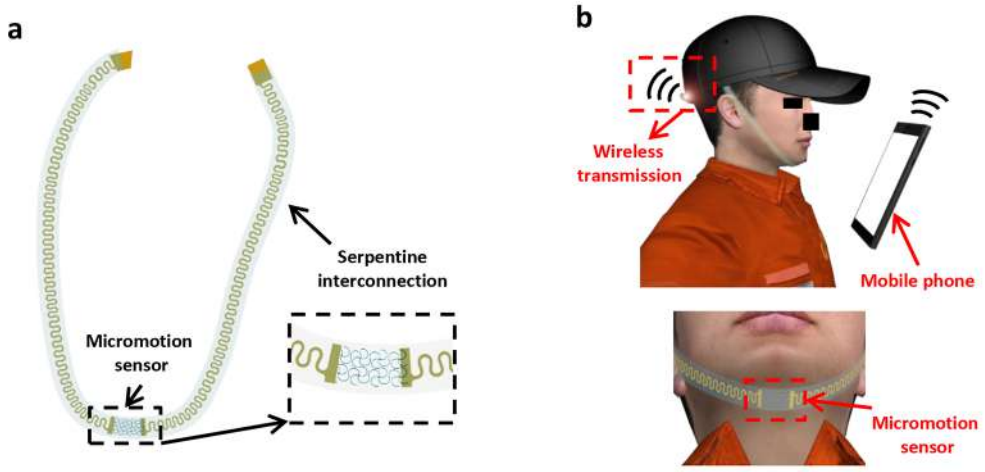

Figure 4. Structural design of the stretchable micromotion sensor with a serpentine layout. (a) Schematic illustration and exploded view schematic diagram of the sensor to be integrated with a wireless data-transmitting module. (b) Schematic diagram of the wireless data-transmitting process from the sensor to a mobile phone.

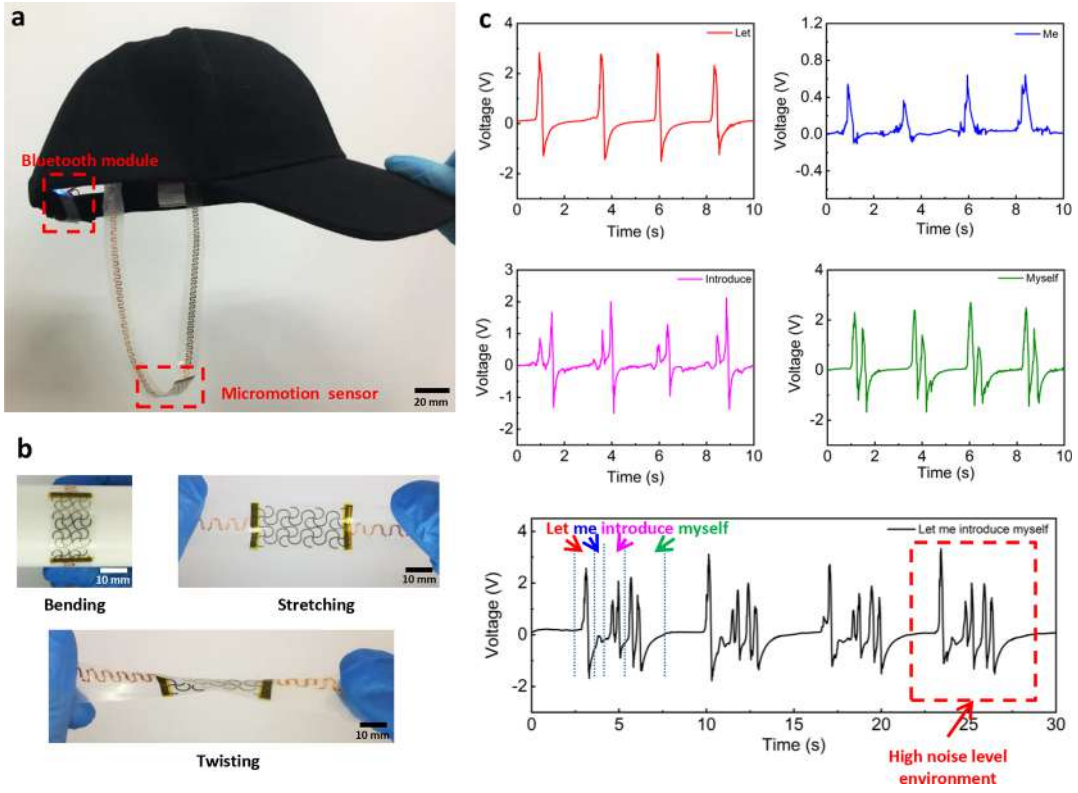

Figure 5. Speech pattern recognition realized by the stretchable micromotion sensor with a serpentine layout. (a) Photograph of the sensor integrated with the wireless data-transmitting module in a wearable system. (b) Photographs of the sensor with different mechanical deformation, including bending, stretching, and twisting. (c) Output voltage signals of the sensor corresponding to the throat or the lower jaw movements of the tester who makes successive "Let", "Me", "Introduce", and "Myself".

configuration of $\theta = 230°$ and $W/L = 0.15$ when the film was cyclically stretched to 12.5% at frequencies up to 4 Hz. As shown in Figure 3f, the output OC voltage remains approximately constant when the frequency is higher than 1 Hz. We also note that the output OC voltage increases with the frequency at frequencies below 1 Hz, which may be attributed to the improved impendence matching due to the frequency dependence of the impendence of the sensor.[44] Similar to the response of the output OC voltage to the frequency, the output SC current remains stable when the stretching frequency is higher than 1 Hz, which is shown in Figure S11, Supporting Information. The experimental results indicate that the micromotion sensor with a serpentine layout possesses a good sensing performance with a stretchability as high as ~30%, demonstrating the feasibility in the applications of epidermal micromotion monitoring.

The stretchable micromotion sensor with the serpentine layout was then integrated with a wireless data transmitting module with the design shown in Figure 4. Figure 4a shows the necklace design used to connect the sensor and the wireless

DOI: 10.1021/acsami.8b22613
ACS Appl. Mater. Interfaces 2019, 11, 12261−12271

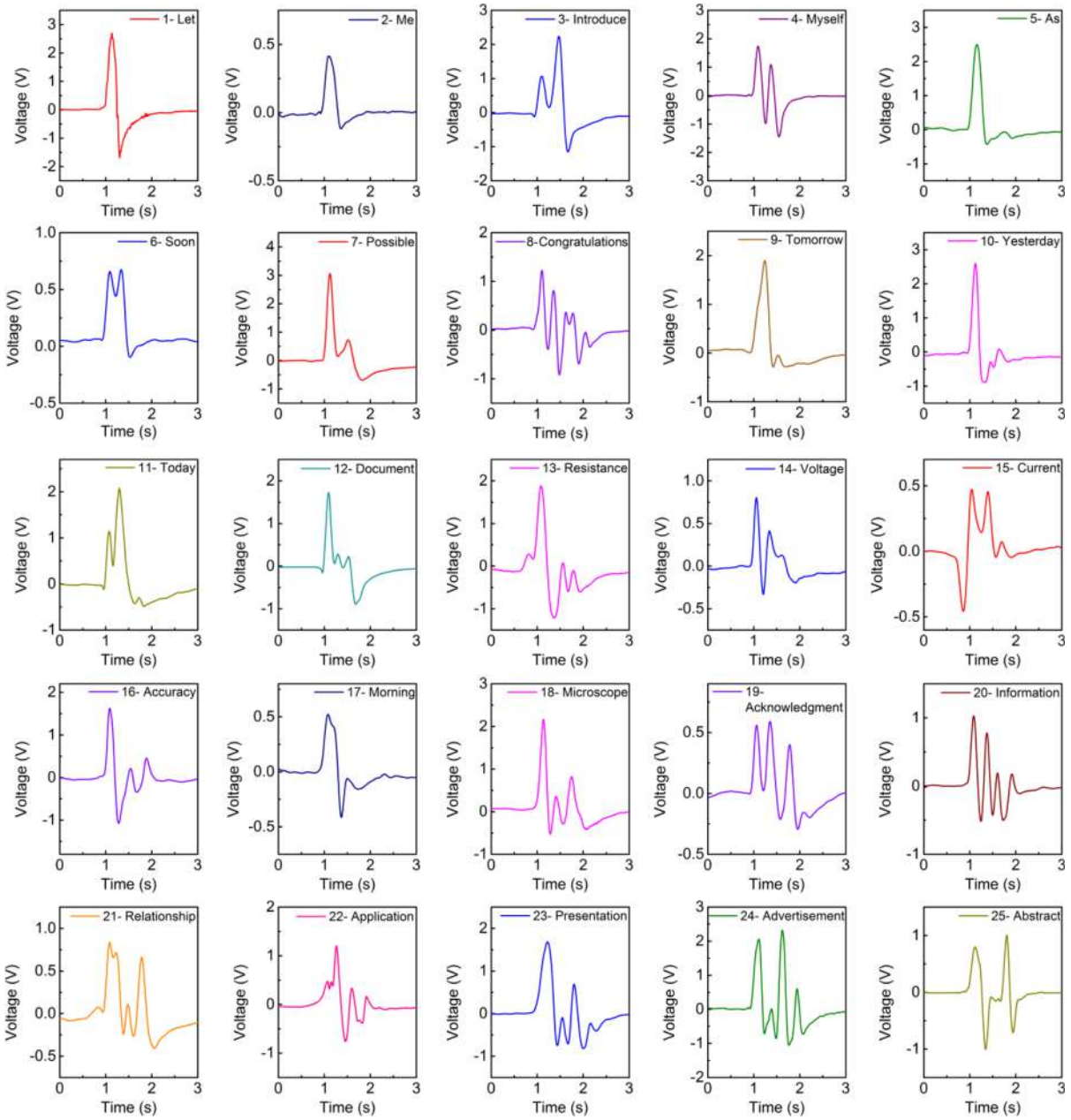

Figure 6. Speech pattern recognition of 25 English words.

module. A long serpentine Cu ribbon encapsulated with a PU film, which was fabricated by physical carving of Cu foil using a cutting machine, served as the interconnects. As illustrated in Figure 4b, after connecting the sensor with the wireless data-transmitting module, which can be embedded in a cap, the sensor is attached to the skin around the lower jaw of a human. When the skin around the throat and the lower jaw moves during speaking, strain is induced into the sensor, and corresponding electrical signals are generated via the piezoelectric effect. Meanwhile, the wireless data-transmitting module acquires and transmits the electrical signals to the wireless terminals like a mobile phone or a laptop. When people are speaking, the movement features of the skin around the throat and the lower jaw are determined by the spoken word. The skin movements depending on the spoken words lead to different dynamic strain distributions on the PVDF layer of the sensor, which generate output electrical signals with various time-domain or frequency-domain features. By analyzing the corresponding electrical signals, the voice recognition can be realized.

Figure 5a and Figure S12 of the Supporting Information illustrate the integration of the stretchable micromotion sensor and a wireless data-transmitting module in experiments. As an example, a baseball cap can be a perfect carrier of the integration. Both ends of the serpentine Cu interconnects are connected to the input interface of the wireless data-transmitting module. As demonstrated in Figure 5b and Figure S13 of the Supporting Information, excellent flexibility and stretchability of the sensor remains after the encapsulation. After the integration, the capability of the sensor to recognize speech pattern is evaluated. In the test, a tester wearing the baseball cap (Figure S14 of the Supporting Information) pronounced some separate words first and then a continuous sentence consisting of these words. As illustrated in Figure S15

DOI: 10.1021/acsami.8b22613
ACS Appl. Mater. Interfaces 2019, 11, 12261−12271

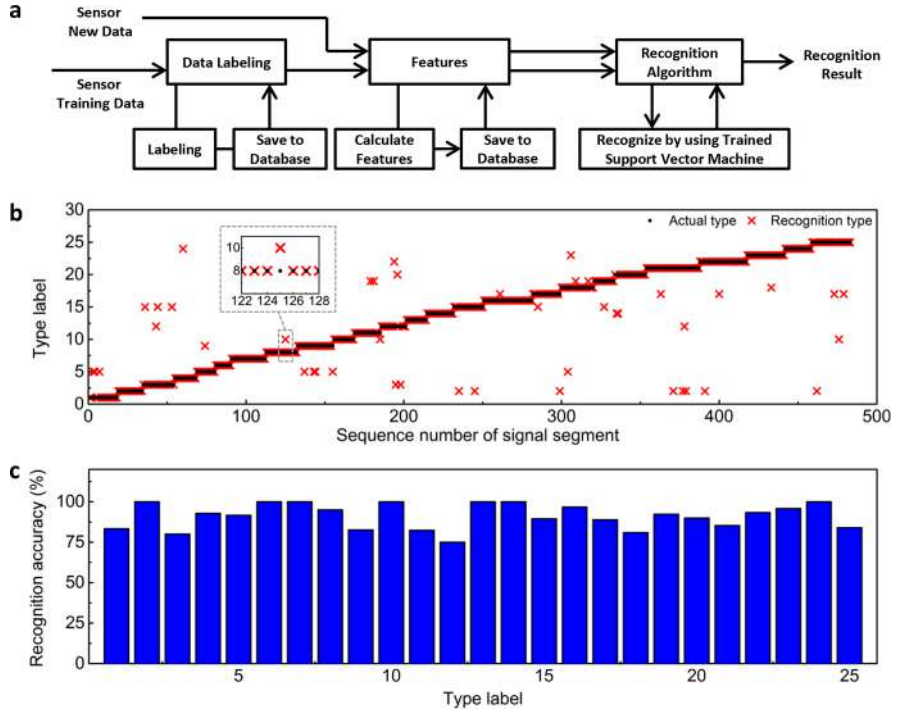

Figure 7. Machine learning based on speech pattern recognition. (a) Flowchart of the working procedure of machine learning. (b) Recognition results of 25 English words. (c) Recognition accuracy of 25 English words.

of the Supporting Information, the voltage signal of the sensor is acquired and transmitted to a mobile phone for recording. Figure 5c presents the results of speech pattern recognition tests. When the tester repeated words including "Let", "Me", "Introduce", and "Myself" separately, a voltage signal up to 2V, which is generated by the sensor, can be collected by the mobile phone without any additional preamplifier. Strong correlation between the voltage signal and the word can be observed by comparing the signal feature of the four words. It can also be noted that the regularity and repeatability of the signal are excellent when repeating each word four times. When the tester repeated the sentence "Let me introduce myself" and the phrase "Introduce me" (Figure S16 of the Supporting Information), the regularity and repeatability of the voltage signal remained good. Further comparison between the voltage signal features of the repeated separate words and the continuous sentence shows that signal features of the pronounced sentence is consistent with the ones of the pronounced separate words. The four words can be identified by matching the signal features of each word in the voltage signals of the sentence. Moreover, the speech pattern recognition performance of the sensor is resistive to the environmental noise. As indicated by Figure 5c, when the environment in which the tester repeated the sentence switched from a quiet one to a noisy one (where a song was played), the voltage signal recorded in the noisy environment was substantially unchanged. These test results clearly indicate that the micromotion sensor with a serpentine mesh geometry is capable for speech pattern recognition in both quiet and noisy environments. Besides, other kinds of human body movements, including coughing, yawning, deglutition, shaking of the head, and nodding, can also be monitored by the mesh-engineered sensor, as shown in Figure S17 of the Supporting Information.

To achieve enhanced performance in voice collection and recognition, the serpentine mesh geometric micromotion sensor should be able to distinguish more English words.[45] Figure 6 demonstrates the output voltage signal waveforms of 25 English words. It can be seen that the waveforms are unique and repeatable for all 25 words. Every specific word has its own different key features, including amplitude, duration, and output voltage variation, which are caused by different movements of the throat or the lower jaw, indicating that these kinds of muscle movements also have recognizable characteristics. Figure S18a of the Supporting Information demonstrate that a similar signal shape can be obtained when a tester pronounces the same word "Myself" with or without vocalization, which could remarkably assist patients who have difficulty in pronunciation. Besides, we test three different people speaking the same English word "Myself." As shown in Figure S18b of the Supporting Information, the micromotion sensors placed in the same position on different people yielded very similar shapes of responses for the word, meaning that it is possible to establish a speech recognition system to recognize different types of words, phrases, and sentences among different people.

The waveforms of test signals can be recognized by a machine learning approach.[45−48] A program based on a support-vector machine (SVM) has been implemented in Matlab to automatically recognize the speech signal from the serpentine mesh geometric micromotion sensor. Figure 7 illustrates the work procedures and results of machine learning recognizing different English words. With the work procedures shown in Figure 7a, 608 signal segments corresponding to different English word shown in Figure 6, were labeled with 1 to 25 according to the word type (the number of each word type is shown in Table S2). Before the recognization, 125 signal segments from them (five per label) were chosen randomly to feed the SVM for training, and the training

DOI: 10.1021/acsami.8b22613
ACS Appl. Mater. Interfaces 2019, 11, 12261−12271

process involved 13 features of signal segments. Then, the remaining signals segments (483 signal segments) were inputted into the trained SVM, and corresponding recognition results were outputted and are demonstrated in Figure 7b,c. As shown in Figure 7b, the red cross mark represents the recognized type via the SVM, and the black dot represents the original signal segment type. The results show that 438 signal segments can be correctly recognized, which represents 90.68% correctness. Because the speech rate is different for everyone, the period of the strain signal associated with the spoken word or phrase can be different. To investigate influence of the period of strain signal on the recognition results, we select the signal segment of "soon" as the object of study. Several characteristic signals with different pulse widths varying from 0.9 to 1.5 times the original pulse width are formed, which are shown in the left panel of Figure S19 of the Supporting Information. Then, these signal patterns are inputted into the trained SVM, and corresponding consequences are illustrated in the right panel of Figure S20 of the Supporting Information. It can be seen that all of them can be recognized by the trained SVM correctly. The results show that when the speakers say the word "soon" slower or faster, the trained SVM is still able to recognize the signal. Moreover, Figure 7c illustrates that the recognition accuracy of each type of word is more than 75%. Thus, the output voltage signals yielded by the serpentine mesh geometric micromotion sensor can be recognized by the machine learning approach.

CONCLUSIONS

In summary, by engineering hard-to-stretch high-performance piezoelectric materials, such as PVDF, with a serpentine layout, a stretchable micromotion sensor that can be used in voice recognition is presented. The experimental results show that the serpentine layout design can offer good stretchability and high sensitivity to the sensor at the same time. With the experimental and computational results, the geometric parameter optimization strategies of the serpentine mesh geometry for piezoelectric materials, when taking output performance and stretchability into account, are discussed. Using the optimized design that can be stretched to 27.5 % and achieve sensitivities of 72 V/ε and 272.73 nA/ε, a wireless stretchable micromotion sensor is fabricated. The capability of the sensor to realize voice recognition, including speech pattern recognition with machine learning, is demonstrated. This study illustrates a broader application of serpentine layout design in using conventional hard-to-stretch high-performance functional materials, not only piezoelectric materials, in the design of novel, flexible, and stretchable electronic devices.

EXPERIMENTAL SECTION

Fabrication of the Stretchable Piezoelectric Micromotion Sensor. The PVDF films with a serpentine layout were fabricated by the laser engraving method (Han's Laser, China). First, the bottom Cu leading wires processed by a physical engraving method (Silhouette Cameo, USA) were transferred to a 30-μm-thick smooth poly(tetrafluoroethylene) (PTFE) membrane. Then, thermal release tape (Revalpha, Nitto Denko) was used to transfer the stretchable PVDF film onto PTFE boards. The bottom metal layer of the PVDF structure should be well aligned to the electric contact sites of the Cu leading wires. The Kapton film was applied to fasten the contact sites. After that, the top Cu leading wires were transferred to the PTFE membrane and aligned to the electric contact sites of the top metal layer in the PVDF film. The polyurethane membrane (47-μm-thick) served as the top encapsulation layer and could pick up the device from the PTFE membrane and print it to another polyurethane membrane with the same thickness.

Finite Element Analysis (FEA). ABAQUS commercial software was employed to study the mechanical properties of the stretchable piezoelectric composite with different dimensions. All parts were modeled by the hexahedron elements (C3D8R). An elastic modulus of 69 GPa and Poisson's ratio of 0.35 described the mechanical behavior of Al. An elastic modulus of 1.47 MPa and Poisson's ratio of 0.34 described the mechanical behavior of PVDF. An elastic modulus of 6.4 MPa and Poisson's ratio of 0.49 described the mechanical behavior of polyurethane. The elastic modulus and Poisson's ratio are 2.5 GPa and 0.34, respectively, for the Kapton film.

Measurements of Electrical and Mechanical Performance. A linear motor (LinMot-B01-37X166/160) was used to conduct the cyclic stretching tests of the stretchable PVDF micromotion sensors (Figure S20 of the Supporting Information). The open-circuit voltage signals of the stretchable piezoelectric unit were measured by using a Keithley 6514 electrometer. The short-circuit current signals of the unit were measured with a low-noise current preamplifier (Stanford Research SR570). Each of the reported data corresponds to an average of measurements of five samples. Young's moduli of different materials and stress–strain curves of the Al/PVDF/Al film were measured using a universal test frame (AGS-X, Shimadzu, Japan), which are shown in Figures S9, S21, and S22 of the Supporting Information.

Speech Pattern Recognition. The parameters c and g of SVM is 2.2 and 1.1, respectively. The other parameters of SVM are default parameters of the Libsvm toolbox in MATLAB software.

ASSOCIATED CONTENT

Supporting Information

The Supporting Information is available free of charge on the ACS Publications website at DOI: 10.1021/acsami.8b22613.

Calculation of the output voltage of the stretchable micromotion sensor with a serpentine layout; optical images, optical micrographs, and plots of open-circuit voltages and corresponding short-circuit currents of the mesh-engineered PVDF films; σ_{11}, σ_{22}, and σ_{33} distributions in the PVDF layer of the sensor; I–V curve and cross-sectional SEM image of the Al/PVDF/Al film; simulated strain distribution in the Al layer of the sensor; stress–strain curves of PVDF and PU; photograph of the wireless data-transmitting module; photograph of the stretchable micromotion sensor and photograph of the tester wearing the sensor; photograph of the experiments of speech pattern recognition; output voltage signals of the sensor caused by the throat or the lower jaw movements of words; and tables of the parameters of the piezoelectric material and label and corresponding number of samples of 25 English words (PDF)

Measurement of OC voltage of sensor (AVI)

Two LEDs driven by the output voltage of the sensor under cyclic stretching load (AVI)

Speech pattern recognition experiment (AVI)

AUTHOR INFORMATION

Corresponding Authors

*E-mail: tspan@uestc.edu.cn (T.P.).
*E-mail: linyuan@uestc.edu.cn (Y.L.).

ORCID

Zhuocheng Yan: 0000-0001-8123-7357
Taisong Pan: 0000-0003-1576-3409
Min Gao: 0000-0003-3899-2933

DOI: 10.1021/acsami.8b22613
ACS Appl. Mater. Interfaces 2019, 11, 12261–12271

Weiqing Yang: 0000-0001-8828-9862
Yuan Lin: 0000-0002-9879-4341

Notes

The authors declare no competing financial interest.

■ ACKNOWLEDGMENTS

Y.L., T.P., and Z.Y. discussed and initiated the study, and Y.L. and T.P. supervised the project. Z.Y. conducted the fabrication experiments. Z.Y. and T.P. conducted the mechanical simulations. Z.Y. and L.J. performed the cycle loading measurement. Z.Y., J.L., J.J., and Z.Q. performed the sound measurement. Z.Y., T.P., D.W., L.J., L.H., J.J., H.Z., M.G., W.Y., and Y.L. analyzed the data and co-wrote the manuscript. All authors reviewed and finalized the manuscript. This work was supported by the National Basic Research Program of China (973 Program) under Grant no. 2015CB351905, the Natural Science Foundation of China (no. 61825102), "111" project (nos. B13042 and B18011), the Fundamental Research Funds for the Central Universities of China (nos. ZYGX2015J140 and ZYGX2016KYQD132), and the Scientific and Technological Projects for Distinguished Young Scholars of Sichuan Province (no. 2015JQ0013).

■ REFERENCES

(1) Huang, Y.; Gao, L.; Zhao, Y.; Guo, X.; Liu, C.; Liu, P. Highly Flexible Fabric Strain Sensor Based on Graphene Nanoplatelet-polyaniline Nanocomposites for Human Gesture Recognition. *J. Appl. Polym. Sci.* **2017**, *134*, 45340.

(2) Guo, X.; Huang, Y.; Zhao, Y.; Mao, L.; Gao, L.; Pan, W.; Zhang, Y.; Liu, P. Highly Stretchable Strain Sensor Based on SWCNTs/CB Synergistic Conductive Network for Wearable Human-activity Monitoring and Recognition. *Smart Mater. Struct.* **2017**, *26*, No. 095017.

(3) Pang, Y.; Tian, H.; Tao, L.; Li, Y.; Wang, X.; Deng, N.; Yang, Y.; Ren, T.-L. Flexible, Highly Sensitive, and Wearable Pressure and Strain Sensors with Graphene Porous Network Structure. *ACS Appl. Mater. Interfaces* **2016**, *8*, 26458−26462.

(4) Tao, L.-Q.; Tian, H.; Liu, Y.; Ju, Z.-Y.; Pang, Y.; Chen, Y.-Q.; Wang, D.-Y.; Tian, X.-G.; Yan, J.-C.; Deng, N.-Q.; Yang, Y.; Ren, T.-L. An Intelligent Artificial Throat with Sound-sensing Ability Based on Laser Induced Graphene. *Nat. Commun.* **2017**, *8*, 14579.

(5) Barker, J.; Marxer, R.; Vincent, E.; Watanabe, S. The Third 'CHIME' Speech Separation and Recognition Challenge: Analysis and Outcomes. *Comput. Speech. Lang.* **2017**, *46*, 605−626.

(6) Wade, J.; Petheram, B.; Cain, R. Voice Recognition and Aphasia: Can Computers Understand Aphasic speech? *Disabil. Rehabil.* **2001**, *23*, 604−613.

(7) Amaya, A.; Woolf, C.; Devane, N.; Galliers, J.; Talbot, R.; Wilson, S.; Marshall, J. Receiving Aphasia Intervention In a Virtual Environment: The Participants' Perspective. *Aphasiology* **2018**, *32*, 538−558.

(8) Li, Y.; Zhou, B.; Zheng, G.; Liu, X.; Li, T.; Yan, C.; Cheng, C.; Dai, K.; Liu, C.; Shen, C.; Guo, Z. Continuously Prepared Highly Conductive and Stretchable SWNT/MWNT Synergistically Composited Electrospun Thermoplastic Polyurethane Yarns for Wearable Sensing. *J. Mater. Chem. C* **2018**, *6*, 2258.

(9) Cai, Y.; Shen, J.; Ge, G.; Zhang, Y.; Jin, W.; Huang, W.; Shao, J.; Yang, J.; Dong, X. Stretchable Ti3C2Tx MXene/Carbon Nanotube Composite Based Strain Sensor with Ultrahigh Sensitivity and Tunable Sensing Range. *ACS Nano* **2018**, *12*, 56−62.

(10) Kim, J.; Lee, M.; Shim, H. J.; Ghaffari, R.; Cho, H. R.; Son, D.; Jung, Y. H.; Soh, M.; Choi, C.; Jung, S.; Chu, K.; Jeon, D.; Lee, S.-T.; Kim, J. H.; Choi, S. H.; Hyeon, T.; Kim, D.-H. Stretchable Silicon Nanoribbon Electronics for Skin Prosthesis. *Nat. Commun.* **2014**, *5*, 5747.

(11) Yu, C.; Zhang, Y.; Cheng, D.; Li, X.; Huang, Y.; Rogers, J. A. All-Elastomeric, Strain-Responsive Thermochromic Color Indicators. *Small* **2014**, *10*, 1266−1271.

(12) Jeong, Y. R.; Kim, J.; Xie, Z.; Xue, Y.; Won, S. M.; Lee, G.; Jin, S. W.; Hong, S. Y.; Feng, X.; Huang, Y.; Rogers, J. A.; Ha, J. S. A Skin-attachable, Stretchable Integrated System Based on Liquid GaInSn for Wireless Human Motion Monitoring with Multi-site Sensing Capabilities. *NPG Asia Mater.* **2017**, *9*, e443.

(13) Liao, X.; Zhang, Z.; Kang, Z.; Gao, F.; Liao, Q.; Zhang, Y. Ultrasensitive and Stretchable Resistive Strain Sensors Designed for Wearable Electronics. *Mater. Horiz.* **2017**, *4*, 502−510.

(14) Muth, J. T.; Vogt, D. M.; Truby, R. L.; Mengüç, Y.; Kolesky, D. B.; Wood, R. J.; Lewis, J. A. Embedded 3D Printing of Strain Sensors within Highly Stretchable Elastomers. *Adv. Mater.* **2014**, *26*, 6307−6312.

(15) Wang, Y.; Wang, L.; Yang, T.; Li, X.; Zang, X.; Zhu, M.; Wang, K.; Wu, D.; Zhu, H. Wearable and Highly Sensitive Graphene Strain Sensors for Human Motion Monitoring. *Adv. Funct. Mater.* **2014**, *24*, 4666−4670.

(16) Frutiger, A.; Muth, J. T.; Vogt, D. M.; Mengüç, Y.; Campo, A.; Valentine, A. D.; Walsh, C. J.; Lewis, J. A. Capacitive Soft Strain Sensors via Multicore-Shell Fiber Printing. *Adv. Mater.* **2015**, *27*, 2440−2446.

(17) Ying, M.; Bonifas, A. P.; Lu, N.; Su, Y.; Li, R.; Cheng, H.; Ameen, A.; Huang, Y.; Rogers, J. A. Silicon Nanomembranes for Fingertip Electronics. *Nanotechnology* **2012**, *23*, 344004.

(18) Yao, S.; Zhu, Y. Wearable Multifunctional Sensors Using Printed Stretchable Conductors Made of Silver Nanowires. *Nanoscale* **2014**, *6*, 2345−2352.

(19) Cai, L.; Song, L.; Luan, P.; Zhang, Q.; Zhang, N.; Gao, Q.; Zhao, D.; Zhang, X.; Tu, M.; Yang, F.; Zhou, W.; Fan, Q.; Luo, J.; Zhou, W.; Ajayan, P. M.; Xie, S. Super-stretchable, Transparent Carbon Nanotube-Based Capacitive Strain Sensors for Human Motion Detection. *Sci. Rep.* **2013**, *3*, 3048.

(20) Lipomi, D. J.; Vosgueritchian, M.; Tee, B. C.-K.; Hellstrom, S. L.; Lee, J. A.; Fox, C. H.; Bao, Z. Skin-like Pressure and Strain Sensors Based on Transparent Elastic Films of Carbon Nanotubes. *Nat. Nanotechnol.* **2011**, *6*, 788−792.

(21) Cohen, D. J.; Mitra, D.; Peterson, K.; Maharbiz, M. M. A Highly Elastic, Capacitive Strain Gauge Based on Percolating Nanotube Networks. *Nano Lett.* **2012**, *12*, 1821−1825.

(22) Dagdeviren, C.; Yang, B. D.; Su, Y.; Tran, P. L.; Joe, P.; Anderson, E.; Xia, J.; Doraiswamy, V.; Dehdashti, B.; Feng, X.; Lu, B.; Poston, R.; Khalpey, Z.; Ghaffari, R.; Huang, Y.; Slepian, M. J.; Rogers, J. A. Conformal Piezoelectric Energy Harvesting and Storage from Motions of the Heart, Lung, and Diaphragm. *Proc. Natl. Acad. Sci. U. S. A.* **2014**, *111*, 1927−1932.

(23) Lu, B.; Chen, Y.; Ou, D.; Chen, H.; Diao, L.; Zhang, W.; Zheng, J.; Ma, W.; Sun, L.; Feng, X. Ultra-flexible Piezoelectric Devices Integrated with Heart to Harvest the Biomechanical Energy. *Sci. Rep.* **2015**, *5*, 16065.

(24) Lü, C.; Wu, S.; Lu, B.; Zhang, Y.; Du, Y.; Feng, X. Ultrathin Flexible Piezoelectric Sensors for Monitoring Eye Fatigue. *J. Micromech. Microeng.* **2018**, *28*, No. 025010.

(25) Kim, Y.-S.; Xie, Y.; Wen, X.; Wang, S.; Kim, S. J.; Song, H.-K.; Wang, Z. L. Highly Porous Piezoelectric PVDF Membrane as Effective Lithium Ion Transfer Channels for Enhanced Self-charging Power Cell. *Nano Energy* **2015**, *14*, 77−86.

(26) Norrix, L. W.; Camarota, K.; Harris, F. P.; Dean, J. The Effects of FM and Hearing Aid Microphone Settings, FM Gain, and Ambient Noise Levels on SNR at the Tympanic Membrane. *J. Am. Acad. Audiol.* **2016**, *27*, 117−125.

(27) Jang, K.-I.; Chung, H. U.; Xu, S.; Lee, C. H.; Luan, H.; Jeong, J.; Cheng, H.; Kim, G.-T.; Han, S. Y.; Lee, J. W.; Kim, J.; Cho, M.; Miao, F.; Yang, Y.; Jung, H. N.; Flavin, M.; Liu, H.; Kong, G. W.; Yu, K. J.; Rhee, S. I.; Chung, J.; Kim, B.; Kwak, J. W.; Yun, M. H.; Kim, J. Y.; Song, Y. M.; Paik, U.; Zhang, Y.; Huang, Y.; Rogers, J. A. Soft Network Composite Materials with Deterministic and Bio-inspired Designs. *Nat. Commun.* **2015**, *6*, 6566.

DOI: 10.1021/acsami.8b22613
ACS Appl. Mater. Interfaces 2019, 11, 12261−12271

(28) Ma, Y.; Feng, X.; Rogers, J. A.; Huang, Y.; Zhang, Y. Design and Application of 'J-shaped' Stress-strain Behavior in Stretchable Electronics: A Review. *Lab Chip* **2017**, *17*, 1689−1704.
(29) Ma, Q.; Cheng, H.; Jang, K.-I.; Luan, H.; Hwang, K.-C.; Rogers, J. A.; Huang, Y.; Zhang, Y. A Nonlinear Mechanics Model of Bio-inspired Hierarchical Lattice Materials Consisting of Horseshoe Microstructures. *J. Mech. Phys. Solids* **2016**, *90*, 179−202.
(30) Lee, C. H.; Ma, Y.; Jang, K.-I.; Banks, A.; Pan, T.; Feng, X.; Kim, J. S.; Kang, D.; Raj, M. S.; McGrane, B. L.; Morey, B.; Wang, X.; Ghaffari, R.; Huang, Y.; Rogers, J. A. Soft Core/Shell Packages for Stretchable Electronics. *Adv. Funct. Mater.* **2015**, *25*, 3698−3704.
(31) Maziz, A.; Concas, A.; Khaldi, A.; Stalhand, J.; Persson, N.-K.; Jager, E. W. H. Knitting and Weaving Artificial Muscles. *Sci. Adv.* **2017**, *3*, No. e1600327.
(32) Jang, K.-I.; Jung, H. N.; Lee, J. W.; Xu, S.; Liu, Y. H.; Ma, Y.; Jeong, J.-W.; Song, Y. M.; Kim, J.; Kim, B. H.; Banks, A.; Kwak, J. W.; Yang, Y.; Shi, D.; Wei, Z.; Feng, X.; Paik, U.; Huang, Y.; Ghaffari, R.; Rogers, J. A. Ferromagnetic, Folded Electrode Composite as a Soft Interface to the Skin for Long-Term Electrophysiological Recording. *Adv. Funct. Mater.* **2016**, *26*, 7281−7290.
(33) Jang, K.-I.; Han, S. Y.; Xu, S.; Mathewson, K. E.; Zhang, Y.; Jeong, J.-W.; Kim, G.-T.; Webb, R. C.; Lee, J. W.; Dawidczyk, T. J.; Kim, R. H.; Song, Y. M.; Yeo, W.-H.; Kim, S.; Cheng, H.; Rhee, S. I.; Chung, J.; Kim, B.; Chung, H. U.; Lee, D.; Yang, Y.; Cho, M.; Gaspar, J. G.; Carbonari, R.; Fabiani, M.; Gratton, G.; Huang, Y.; Rogers, J. A. Rugged and Breathable Forms of Stretchable Electronics with Adherent Composite Substrates for Transcutaneous Monitoring. *Nat. Commun.* **2014**, *5*, 4779.
(34) Huang, X.; Liu, Y.; Cheng, H.; Shin, W.-J.; Fan, J. A.; Liu, Z.; Lu, C.-J.; Kong, G.-W.; Chen, K.; Patnaik, D.; Lee, S.-H.; Hage-Ali, S.; Huang, Y.; Rogers, J. A. Materials and Designs for Wireless Epidermal Sensors of Hydration and Strain. *Adv. Funct. Mater.* **2014**, *24*, 3846−3854.
(35) Wan, C.; Bowen, C. R. Multiscale-structuring of Polyvinylidene Fluoride for Energy Harvesting: The Impact of Molecular-, Micro- and Macro-structure. *J. Mater. Chem. A* **2017**, *5*, 3091−3128.
(36) Zhang, H.; Xie, Y.; Li, X.; Huang, Z.; Zhang, S.; Su, Y.; Wu, B.; He, L.; Yang, W.; Lin, Y. Flexible Pyroelectric Generators for Scavenging Ambient Thermal Energy and as Self-powered Thermo-sensors. *Energy* **2016**, *101*, 202−210.
(37) Cha, S. N.; Seo, J.-S.; Kim, S. M.; Kim, H. J.; Park, Y. J.; Kim, S.-W.; Kim, J. M. Sound-driven Piezoelectric Nanowire-based Nanogenerators. *Adv. Mater.* **2010**, *22*, 4726−4730.
(38) Siddiqui, S.; Kim, D.-I.; Roh, E.; Duy, L. T.; Trung, T. Q.; Nguyen, M. T.; Lee, N.-E. A Durable and Stable Piezoelectric Nanogenerator with Nanocomposite Nanofibers Embedded in an Elastomer under High Loading for a Self-powered Sensor System. *Nano Energy* **2016**, *30*, 434−442.
(39) Jeong, J.-W.; Kim, M. K.; Cheng, H.; Yeo, W.-H.; Huang, X.; Liu, Y.; Zhang, Y.; Huang, Y.; Rogers, J. A. Capacitive Epidermal Electronics for Electrically Safe, Long-Term Electrophysiological Measurements. *Adv. Healthcare Mater.* **2014**, *3*, 642−648.
(40) Zhang, Y.; Wang, S.; Li, X.; Fan, J. A.; Xu, S.; Song, Y. M.; Choi, K.-J.; Yeo, W.-H.; Lee, W.; Nazaar, S. N.; Lu, B.; Yin, L.; Hwang, K.-C.; Rogers, J. A.; Huang, Y. Experimental and Theoretical Studies of Serpentine Microstructures Bonded To Prestrained Elastomers for Stretchable Electronics. *Adv. Funct. Mater.* **2014**, *24*, 2028−2037.
(41) Kobayashi, T.; Yamashita, T.; Makimoto, N.; Takamatsu, S.; Itoh, T. In Ultra-thin Piezoelectric Strain Sensor 5× 5 Array Integrated on Flexible Printed Circuit for Structural Health Monitoring by 2D Dynamic Strain Sensing, *Micro Electro Mechanical Systems (MEMS)*, 2016 IEEE 29th International Conference on, IEEE: 2016; pp 1030-1033.
(42) Xing, L.; Zhu, R.; Wang, Z.; Wang, F.; Kimura, H. Flexible Tensile Strain Sensor Based on Leadfree 0.5Ba $(Ti_{0.8}Zr_{0.2})$ O_3−0.5$(Ba_{0.7}Ca_{0.3})$ TiO_3 Piezoelectric Nanofibers. *Smart Mater. Struct.* **2017**, *26*, No. 097001.
(43) Lin, L.; Jing, Q.; Zhang, Y.; Hu, Y.; Wang, S.; Bando, Y.; Han, R. P. S.; Wang, Z. L. An Elastic-spring-substrated Nanogenerator as an Active Sensor for Self-powered Balance. *Energy Environ. Sci.* **2013**, *6*, 1164−1169.
(44) Chang, C.; Tran, V. H.; Wang, J.; Fuh, Y.-K.; Lin, L. Direct-write Piezoelectric Polymeric Nanogenerator with High Energy Conversion Efficiency. *Nano Lett.* **2010**, *10*, 726−731.
(45) Wang, Y.; Yang, T.; Lao, J.; Zhang, R.; Zhang, Y.; Zhu, M.; Li, X.; Zang, X.; Wang, K.; Yu, W.; Jin, H.; Wang, L.; Zhu, H. Ultra-sensitive Graphene Strain Sensor for Sound Signal Acquisition and Recognition. *Nano Res.* **2015**, *8*, 1627−1636.
(46) Chang, Y.-W.; Hsieh, C.-J.; Chang, K.-W.; Ringgaard, M.; Lin, C.-J. Training and Testing Low-degree Polynomial Data Mappings via Linear SVM. *J. Mach. Learn. Res.* **2010**, *11*, 1471−1490.
(47) Fan, R.-E.; Chen, P.-H.; Lin, C.-J. Working Set Selection Using Second Order Information for Training Support Vector Machines. *J. Mach. Learn. Res.* **2005**, *6*, 1889−1918.
(48) Chang, C.-C.; Lin, C.-J. *LIBSVM: A Library for Support Vector Machines*. ACM: 2011; p 1-27.

DOI: 10.1021/acsami.8b22613
ACS Appl. Mater. Interfaces 2019, 11, 12261−12271